Effect of transition metal elements on the structural and optical properties of ZnO nanoparticles

I KAZEMINEZHAD[1], S SAADATMAND[1] and RAMIN YOUSEFI[2,*]

[1]Nanotechnology Laboratory, Physics Department, Shahid Chamran University of Ahvaz, Ahvaz, Iran
[2]Department of Physics, Islamic Azad University (IAU), Masjed-Soleiman Branch, Masjed-Soleiman, Iran

Abstract. Undoped and transition metal (TM)-doped ZnO nanoparticles ($Zn_{0.98}X_{0.02}O$-NPs, X = Mn, Cr, Co and Fe) were synthesized from a metal nitrate precursor and gelatin by a sol–gel method. The compounds were synthesized at calcination temperatures of 550°C for 6 h. The synthesized undoped/doped ZnO-NPs were characterized by X-ray diffraction analysis (XRD) and scanning electron microscopy (SEM). XRD results indicated that the sample products were crystalline with a hexagonal wurtzite phase. SEM images showed the ZnO-NPs nearly spherical shapes and a non-uniform shape for doped ZnO-NPs. The crystalline development in the ZnO-NPs was investigated by X-ray peak broadening. The size–strain plot (SSP) method was used to study the individual contributions of crystallite sizes and lattice strain of the undoped and doped ZnO-NPs. The obtained results showed that strain of the NPs plays an important role in peak broadening; moreover, the mean crystalline size of the undoped and doped ZnO-NPs estimated from the SEM and the SSP method was highly inter-correlated. Finally, optical properties of the samples were studied by a UV–Vis spectrometer.

Keywords. TM-doped ZnO-NPs; sol–gel method; size–strain method; optical properties.

1. Introduction

ZnO is an *n*-type semiconductor with high electron mobility, a direct energy band-gap of 3.37 eV and a high exciton binding energy of 60 meV, which is greater than the thermal energy at room temperature. ZnO has numerous attractive characteristics for electronics and optoelectronics devices due to its various accessibility of growth method and also due to its unique properties. ZnO has a good transparency and strong room temperature luminescence, so it can be considered as a promising material for different applications [1–4]. One of the best ways to improve ZnO nanostructure properties is doping. Therefore, to obtain better crystallization quality, optical, electrical and ferromagnetic properties, researchers have studied the effect of dopant materials on ZnO properties. Different reports noted that the role of the particle size, impurities, morphology, the metal oxide host system, surface defects, dopant type and dopant concentration are very important to physical properties and applications of ZnO [5,6]. TM-doped ZnO can be used as magnetic materials with several applications. Therefore, study about effects of these elements on structure and optical properties of ZnO are very important for future applications. In addition, to achieve ZnO nanoparticles with specific property and application, it is necessary to select one of the several growth methods such as sol–gel [7,8], precipitation [9],

solo-chemical processes [10], vapour phase transport (VPT) [11], spray pyrolysis [12], DC thermal plasma synthesis [13], hydrothermal synthesis [14] and chemical vapour deposition (CVD) [15].

In this study, a simple sol–gel method was used to synthesize undoped and TM-doped ZnO-NPs with a narrow size distribution. The strain of the TM-doped ZnO-NPs was calculated using the SSP method. Then, the effects of the strain on the crystallinity and optical properties of ZnO-NPs were investigated.

2. Experimental

To prepare $Zn_{0.98}TM_{0.02}O$-NPs, zinc nitrate hexahydrate ($Zn(NO_3)_2 \cdot 6H_2O$), cobalt nitrate hexahydrate ($Co(NO_3)_2 \cdot 6H_2O$), manganese nitrate hexahydrate ($Mn(NO_3)_2 \cdot 6H_2O$), iron nitrate ($Fe(NO_3)_3 \cdot 9H_2O$), chromium nitrate ($Cr(NO_3)_3 \cdot 9H_2O$), gelatin (($NHCOCH$-$R_1)_n$, R_1 = amino acid) and deionized (DI) water were used as starting materials. To prepare $Zn_{0.98}TM_{0.02}O$-NPs, the specific amounts of zinc nitrate and transition metal nitrate were dissolved in 30 ml of DI water and stirred for 30 min. Meanwhile, 10 g of gelatin was dissolved in 150 ml of DI water and stirred for 30 min at 60°C to achieve a clear gelatin solution. Then, zinc nitrate and transition metal nitrate solution were added to the gelatin solution and the container was moved to a thermostatic oil bath with adjusted temperature at 80°C. The compound solution was then stirred for 12 h to obtain a honey-like resin. The resin became hard after the temperature of the container was

*Author for correspondence (Yousefi.ramin@gmail.com, raminyousefi@iaumis.ac.ir)

reduced to room temperature. The final product was calcined at 500°C in air for 6 h to achieve $Zn_{0.98}TM_{0.02}O$-NPs.

XRD (Philips, X'Pert, $CuK\alpha$) was used to evaluate phase characteristics of the samples. The morphology of the NPs was studied using a scanning electron microscope (SEM, Quanta 200F). Elemental analyses of the products were undertaken using field emission Auger electron spectroscopy (FEAES, JAMP-9500F). UV–Vis spectroscopy (Perikin-Elmer spectrometer) was applied for considering the optical properties. Raman measurements (Jobin Yvon Horiba HR 800 UV) were carried out to study the crystallinity of the obtained products.

3. Results and discussions

Figure 1 shows typical SEM images of the undoped (figure 1a), Fe-doped (figure 1b), Cr-doped (figure 1c), Co-doped (figure 1d) and Mn-doped (figure 1e) ZnO-NPs. As the figures show that the shape of the particles is approximately spherical with uniform size distribution. The size histograms of the ZnO-NPs are shown in figure 2. According to these histograms, the average size of around 105 nm for the undoped and Cr-doped ZnO, 90 nm for Co- and Mn-doped and 96 nm for the Fe-doped ZnO-NPs.

Figure 3a shows the XRD patterns of the undoped and TM-doped ZnO-NPs. The XRD patterns are in agreement with the standard card of ZnO wurtzite hexagonal structure (JCPDS no. 792205). Further, the XRD patterns of all samples show no extra peak due to either any impurity or dopant compounds. The preferred orientation of all XRD patterns of TM-doped ZnO nanoparticles is (101). A slight shift towards the higher degree which is observed in the Cr-, Fe- and Co-doped samples in comparison to that of the undoped ZnO-NPs, while this shift occurs towards the lower degree for Mn-doped sample (figure 3b). The existence of these shifts is related to the difference between the ionic radii of the substitutes (Cr^{+2} (0.63 Å), Co^{+2} (0.72 Å), Fe^{+2} (0.64 Å) and Mn^{+2} (0.80 Å)) [6] with that of Zn^{+2} (0.74 Å). These results are indirect evidence to prove the fact that some of the Zn^{+2} ions have been replaced by TM ions.

Wurtzite lattice parameters such as the values of d, the distance between adjacent planes in the Miller indices ($h\,k\,l$) (calculated from the Bragg equation, $\lambda = 2d\sin\theta$), lattice constants a, b and c, inter-planar angle (φ) and unit cell volumes were calculated from the lattice geometry equation [16]. The lattice parameters of the samples are summarized in table 1. The Scherrer equation is a common method to calculate crystallite size: $D = (k\lambda/\beta_{hkl}\cos\theta)$, where D is the
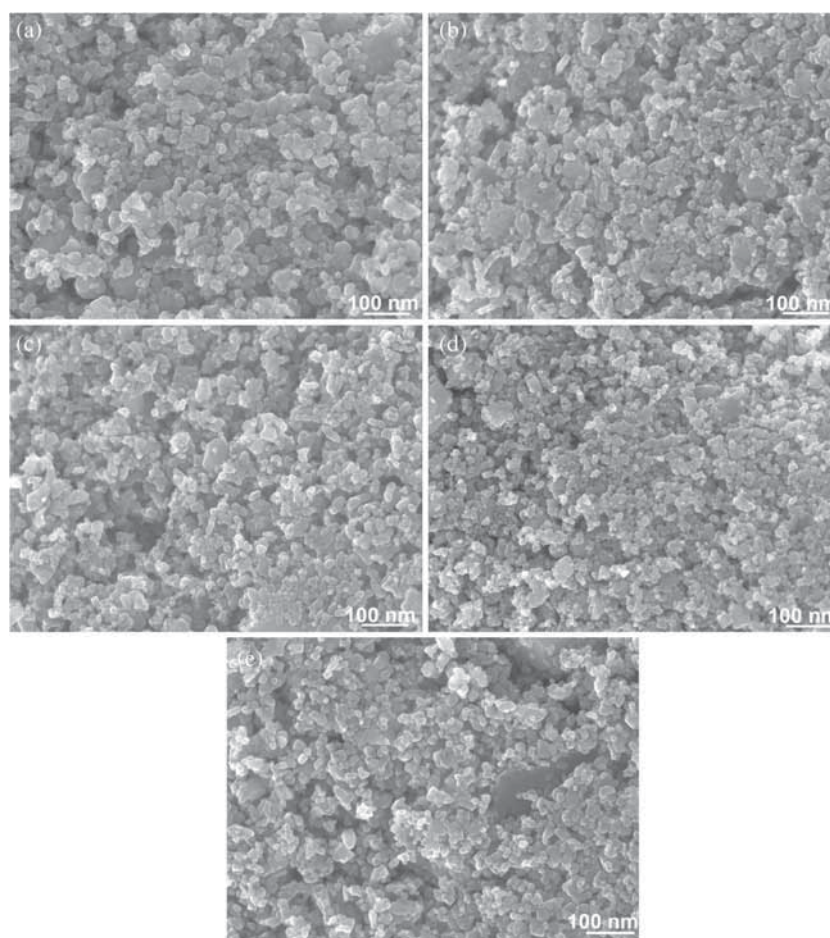

Figure 1. SEM image of (**a**) undoped, (**b**) Fe-doped, (**c**) Cr-doped, (**d**) Co-doped and (**e**) Mn-doped ZnO-NPs.
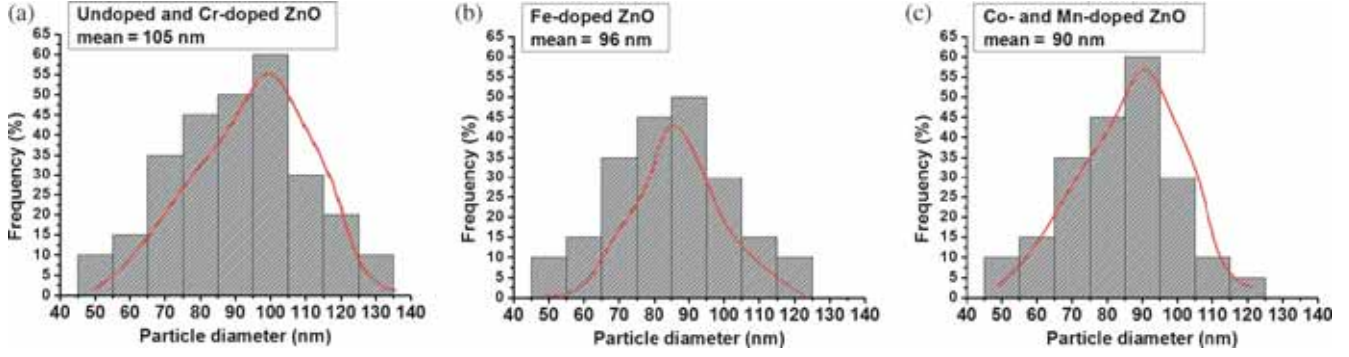
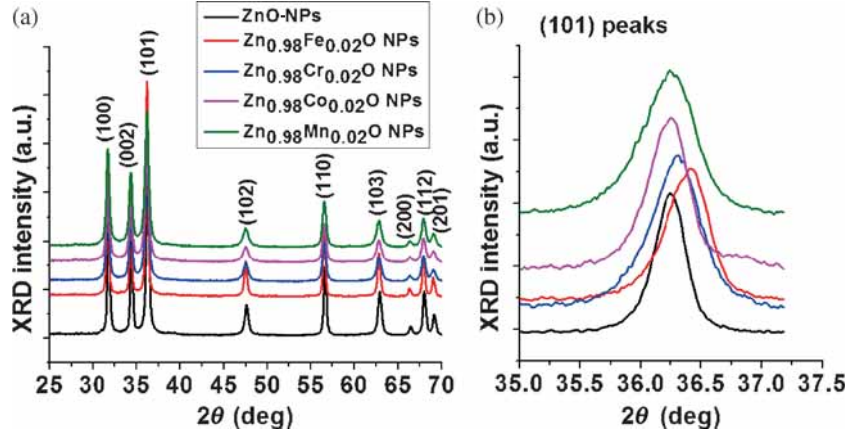**Figure 2.** Diameter size distribution histograms of the NPs.

Figure 3. (**a**) XRD patterns of the undoped and TM-doped ZnO-NPs. (**b**) The (101) peaks of the samples.

Table 1. Calculated lattice constants and crystallite size of grown pure ZnO and TM-doped ZnO at 500°C using XRD patterns.

Sample	FWHM (101) (degree)	Peak position (degree)	Inter-planar spacing (Å) for (101)	Crystallite size (Å) (Scherrer equation)	Lattice parameter (Å)	Crystallite size (Å) SSP method	$\varepsilon \times 10^{-4}$
ZnO	0.29	36.244	2.4787	47.52	$a = 3.2500$ and $c/a = 1.60$	84.26	2.94
$Zn_{0.98}Fe_{0.02}O$	0.31	36.306	2.474	44.44	$a = 3.2418$ and $c/a = 1.61$	70.75	3.18
$Zn_{0.98}Cr_{0.02}O$	0.32	36.410	2.468	47.70	$a = 3.2345$ and $c/a = 1.62$	96.15	3.23
$Zn_{0.98}Co_{0.02}O$	0.36	36.250	2.478	38.27	$a = 3.2518$ and $c/a = 1.60$	58.59	2.95
$Zn_{0.98}Mn_{0.02}O$	0.40	36.241	2.479	34.45	$a = 3.2499$ and $c/a = 1.60$	60.48	3.14

crystallite size in nanometres, λ the wavelength of the radiation (1.54056 Å for CuKα radiation), k a constant equal to 0.94, β_{hkl} the peak width at half-maximum intensity and θ the peak position. According to the Scherrer equation, crystallite size is sorted: $D_{\text{Cr-doped}} > D_{\text{undoped}} > D_{\text{Fe-doped}} > D_{\text{Co-doped}} > D_{\text{Mn-doped}}$.

It is known that some parameters affect the peak width and the most important of these parameters is lattice strain. There are a number of methods used to calculate the effect of lattice strain on broadening of the lattice diffraction peaks such as the Williamson–Hall and size–strain plot (SSP) methods [16]. The SSP method is more accurate, especially at higher diffraction angles. Therefore, the crystallite size and lattice

strain of the samples are calculated using SSP method. In this method, the peak broadening due to the lattice strain is estimated from $\varepsilon = \beta_s / \tan \theta$ [16]. Therefore, the total broadening is obtained from

$$\beta_{hkl} = \beta_s + \beta_D, \tag{1}$$

where β_D is the peak broadening that is corresponding to crystallite size. According to the SSP method, the relation between lattice strain and crystallite size is given by:

$$(d_{hkl}\beta_{hkl}\cos\theta)^2 = \frac{A}{D}\left(d_{hkl}^2\beta_{hkl}\cos\theta\right) + \left(\frac{\varepsilon}{2}\right)^2, \tag{2}$$

where A is a constant, equal to 3/4 for the spherical shape samples used in this experiment. In figure 4, the term $(d\beta \cos\theta)^2$ is plotted with respect to $(d^2\beta \cos\theta)$ for all the diffraction peaks of undoped and TM-doped ZnO-NPs from $2\theta = 25$–$70°$. The crystallite size and strain can be obtained from the slope and root of the y-intercept of the linearly fit data, respectively. According to SSP method, the crystallite size and strain of the NPs are sorted: $D_{\text{Cr-doped}} > D_{\text{undoped}} > D_{\text{Fe-doped}} > D_{\text{Mn-doped}} > D_{\text{Co-doped}}$ and $\varepsilon_{\text{Cr-doped}} > \varepsilon_{\text{Fe-doped}} >$

$\varepsilon_{\text{Mn-doped}} > \varepsilon_{\text{Co-doped}} > \varepsilon_{\text{ZnO}}$. It can be seen that the arrangement of D is approximately the same in two methods. Furthermore, this arrangement is in good agreement with the SEM images. In addition, Cr with smaller ionic radius creates bigger strain in comparison to the other samples.

Figure 5a–d shows results of high-resolution N(E) Auger electron spectroscopy of Cr, Fe, Mn and Co, respectively. As illustrated in figure 5a, two Cr peaks at 476 and 485 eV are evident for the Cr-doped ZnO-NPs. These correspond
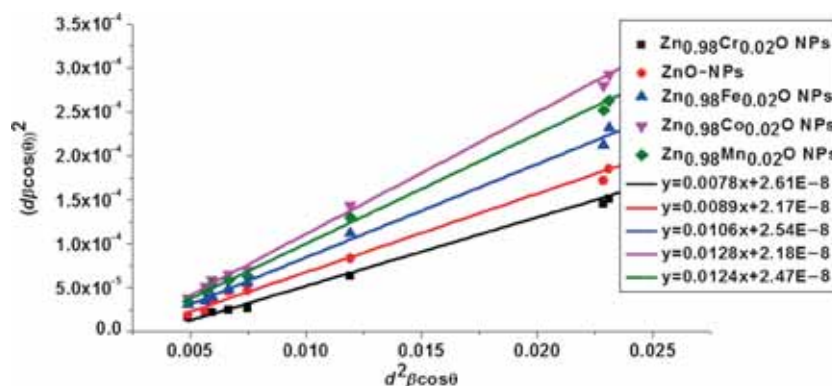

Figure 4. SSP plot of the undoped and TM-doped ZnO-NPs. The crystallite size is achieved from the slope of the linearly fit data, while the root of the y-intercept gives the strain.
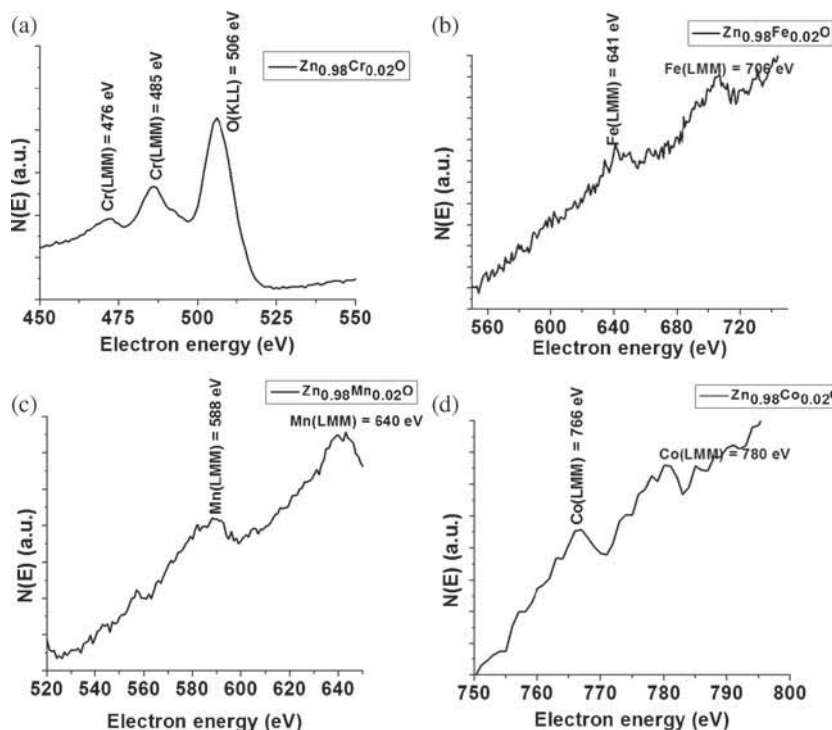

Figure 5. High-resolution N(E) Auger electron emission spectroscopy of the TM-doped ZnO nanoparticles: (**a**) chromium spectrum, (**b**) iron spectrum, (**c**) manganese spectrum and (**d**) cobalt spectrum corresponding to LMM Auger electron emissions from chromium, iron, manganese and cobalt, respectively.
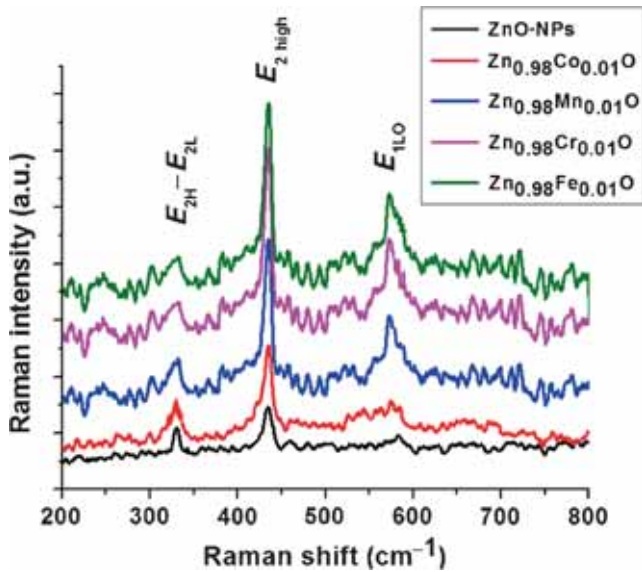
Figure 6. Raman spectra of the undoped and TM-doped ZnO-NPs.

to MLL Auger electron emissions from the chromium. Figure 5b shows two peaks at 641 and 706 eV that indicate MLL Auger electron emissions from the iron. The FEAES spectrum of Mn-doped ZnO-NPs is shown in figure 5c. It also includes two peaks at 588 and 640 eV that correspond to LMM Auger electron emission from manganese. FEAES spectrum of Co-doped also reveals two peaks at 766 and 780 eV that belong to LMM Auger electron emission from cobalt. The FEAES results show that the concentrations of dopant materials are the same for all samples. Such peaks from the FEAES and XRD results provide strong evidence for successful Cr-, Fe-, Mn- and Co-doped in ZnO-NPs.

Raman scattering at room temperature was carried out to investigate the vibrational mode and influence of TM doping on ZnO nanostructure. Raman spectroscopy is an effective technique for estimating the crystallinity of materials. According to the group theory, single crystalline ZnO belongs to the C_{6V}^4 (P63mc) space group, having two formula units per primitive cell and eight sets of optical phonon modes
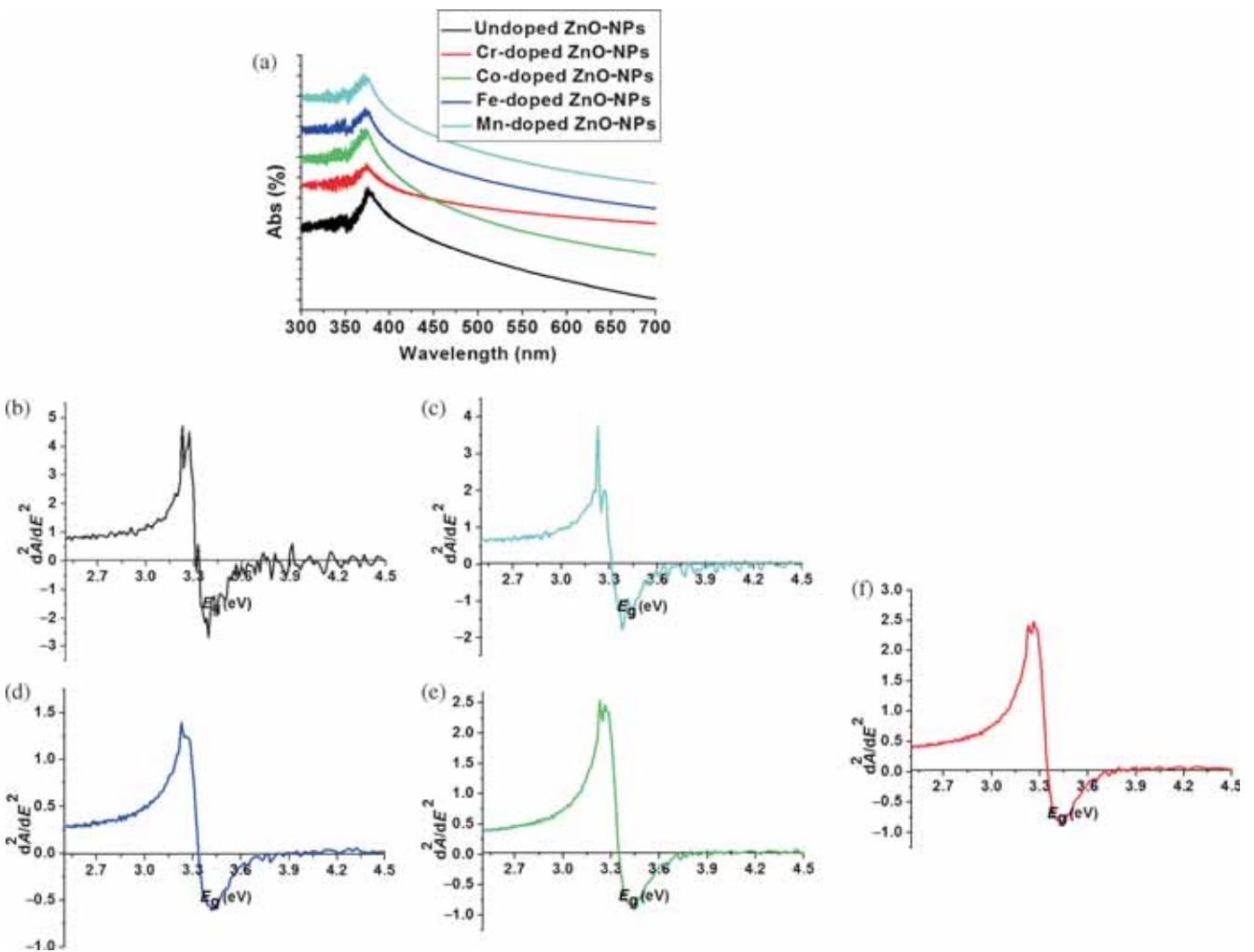

Figure 7. (**a**) Second derivative of the UV–Vis absorption spectra of the undoped and TM-doped ZnO-NPs. (**b–f**) The band gap of the undoped and TM-doped ZnO-NPs estimated from second derivate and energy excel intersect.

at the Γ point of the Brillouin zone (BZ). The phonon modes at the BZ centre for hexagonal structure are given by:

$$\Gamma = 2A_1 + 2E_1 + 2E_2 + 2B_1, \tag{3}$$

which is $A_1 + E_1 + 2E_2$ modes are Raman active, $A_1 + E_1$ modes are infrared (IR) active and B_1 modes are silent (neither Raman nor IR active). The A_1 mode is polarized parallel to the C-axis and the E_1 mode is polarized perpendicular to the C-axis, and both split into transverse optical (TO) and longitudinal optical (LO) branches; the E_{2H}–E_{2L} mode exhibits the presence of undoped ZnO that can only be found when the ZnO is a single crystal. The E_2 (high) mode of the Raman active mode is a characteristic peak for the wurtzite hexagonal phase of ZnO. The E_1 (LO) mode is associated with impurities and formation defects such as oxygen vacancies. The Raman spectra of nanoparticles with different TM dopants are shown in figure 6. The peaks around 330 cm^{-1} for different dopant indicates the E_{2H}–E_{2L} (multi-phonon process) mode, which determines that the nanoparticles are single crystals. This peak for Mn-doped ZnO-NPs is sharper in comparison with the other samples indicating that most of the Mn-doped ZnO-NPs are single crystals. All spectra show a sharp and strong peak at around 434 cm^{-1} that is assigned to E_2 (high) mode and it is a characteristic peak of wurtzite hexagonal ZnO, confirming that the TM-doped ZnO-NPs have wurtzite hexagonal structure. The peak at 572.524, 574.115, 583.149 and 583.149 for Fe, Co, Cr and Mn, respectively, are referred to be E_1 (LO) mode, confirming associated with the impurities and formation of defects such as oxygen vacancies that are increased by incorporating dopant. Thus, doped ZnO-NPs with Cr, Co, Fe and Mn enhanced the oxygen vacancies. In fact, the Raman results show more oxygen vacancies for the samples with bigger strain.

The UV–Vis absorption spectra of the ZnO-NPs at room temperature are shown in figure 7a. The spectra reveal a characteristic absorption peak for ZnO at wavelengths from 376 for the undoped ZnO to 373 nm for the doped. This can be attributed to the intrinsic band-gap absorption of ZnO, owing to the electronic transitions from the valence band to the conduction band ($O_{2p} \rightarrow Zn_{3d}$). In addition, the direct band gap can be estimated from the maximum of the first derivative of the absorbance plot *vs*. energy also from intersection of the second derivative with energy axle as shown in figure 7b–f [17]. It can be seen that absorption peak is blue-shifted due to TM element. In fact, these elements as metal can increase electron concentration that cause to widen the band gap of ZnO-NPs.

4. Conclusion

Undoped and TM-doped ZnO-NPs were synthesized by the sol–gel method in gelatin media. The XRD results showed that all of the undoped and doped ZnO-NPs exhibited the hexagonal with a wurtzite structure. The SSP method and Scherrer equation showed the same arrangement for crystallite size of the samples that was in good agreement with the SEM results. In addition, the SSP results indicated a bigger strain and smaller strain for the Cr- and Co-doped ZnO-NPs, respectively. The Raman results revealed that bigger strain caused to create more oxygen vacancy in the ZnO structure. Furthermore, the UV peaks of the TM-doped ZnO-NPs showed a blue-shift in comparison to the undoped ZnO-NPs. This blue-shift could show the donor behaviour of TM elements in ZnO lattice.

References

[1] Azarang M, Shuhaimi A, Yousefi R and Sookhakian M 2015 *RSC Adv.* **5** 21888

[2] Azarang M, Shuhaimi A, Yousefi R and Sookhakian M 2014 *J. Appl. Phys.* **116** 084307

[3] Özgür Ü, Alivov YaI, Liu C, Teke A, Reshchikov M A, Doğan S *et al* 2005 *J. Appl. Phys.* **98** 041301

[4] Jamali-Sheini F, Yousefi R, Joag D S and More M A 2013 *Mater. Lett.* **111** 181

[5] Yousefi R 2015 *Cryst. Eng. Comm.* **17** 2698

[6] Anghel J, Thurber A, Tenne D A, Hanna C B and Punnoosea A 2010 *J. Appl. Phys.* **107** 09E314

[7] Khorsand Zak A, Majid W H A, Darroudi M and Yousefi R 2011a *Mater. Lett.* **65** 70

[8] Omri K, Najeh I, Dhahri R, El Ghoul J and El Mir L 2014 *Microelectron. Eng.* **128** 53

[9] Sahai A and Goswami N 2007 *Ceram. Int.* **40** 14569

[10] Vaezi M R and Sadrnezhaad S K 2007 *Mater. Des.* **28** 515

[11] Jamali-Sheini F, Yousefi R, Sa'aedi A and Huang N M 2014 *Ceram. Int.* **40** 7737

[12] Park S B and Kang Y C 1997 *J. Aerosol. Sci.* **28** S473

[13] Ko T S, Yang S, Hsu H C, Chu C P, Lin H F, Liao S C *et al* 2006 *Mater. Sci. Eng. B* **134** 54

[14] Zhou Y, Liu C, Zhong X, Wu H, Li M and Wang L 2014 *Ceram. Int.* **40** 10415

[15] Yousefi R, Muhamad M R and Khorsand Zak A 2010 *Thin Solid Films* **518** 5971

[16] Khorsand Zak A, Majid W H A, Abrishami M E and Yousefi R 2011b *Solid State Sci.* **13** 251

[17] Khorsand Zak A, Razali R, Majid W H A and Darroudi M 2011 *Int. J. Nanomed.* **6** 1399